

# Magnetic moments of the $N(1535)$ resonance in the chiral unitary model

T. Hyodo,<sup>1</sup> S. I. Nam,<sup>1,2</sup> D. Jido,<sup>1,\*</sup> and A. Hosaka<sup>1</sup>

<sup>1</sup>*Research Center for Nuclear Physics (RCNP), Ibaraki, Osaka 567-0047, Japan*

<sup>2</sup>*Department of Physics, Pusan National University, Pusan 609-735, Korea*

(Dated: October 31, 2018)

We calculate the magnetic moments of the  $N(1535)$  resonance using the chiral unitary model, where the resonance is dynamically generated in the scatterings of the lowest-lying mesons and baryons. We obtain the magnetic moments of the resonance as  $+1.1$  and  $-0.25$  for  $p(1535)$  and  $n(1535)$ , respectively, in units of the nuclear magneton. We discuss the origin of these numbers within the chiral unitary model, then we compare the present results with those of the quark model and the chiral doublet model. The possibility to observe the magnetic moments in experiments is also investigated.

PACS numbers: 12.39.Fe, 14.20.Gk, 13.40.Em

Keywords: chiral unitary approach, magnetic moments, meson-baryon scatterings

## I. INTRODUCTION

The study of the properties of baryon resonances has attracted continuous attention and is one of the most important topics in hadron physics. The first nucleon resonance with the negative parity,  $N(1535)$ , has unique feature of its strong coupling to the  $\eta N$  state, which allows us to take relatively clean data to other resonance regarding the eta meson in the final state as a probe of the intermediate  $N(1535)$ . Theoretically hadronic resonances have been investigated in recent lattice calculations [1, 2, 3], and direct comparison with QCD is becoming possible. On the other line, the property of the negative parity resonance could be related to chiral symmetry of QCD, in particular, to symmetry restoration at finite temperature and density, as reported in the linear representations of chiral symmetry for the resonance [4, 5, 6].

Recently, the chiral unitary model has been successfully applied to meson-baryon scatterings and to the description of the  $s$ -wave baryon resonances as dynamically generated objects by the ground state mesons and baryons [7, 8, 9, 10, 11, 12]. For instance,  $\Lambda(1405)$  being treated as a  $\bar{K}N$  and  $\pi\Sigma$  state reproduces well experimental data available now. Further,  $N(1535)$  and other states in low lying  $J^P = 1/2^-$  states are also discussed in the same framework [13, 14, 15].

In order to investigate the electromagnetic structure of the dynamically generated resonances, in Ref. [16], the magnetic moments were calculated for  $\Lambda(1405)$  and  $\Lambda(1670)$  in the chiral unitary model. Following that paper, we will here calculate the magnetic moments of another  $J^P = 1/2^-$  resonance state,  $N(1535)$ , in the chiral unitary model. Recently, the resonance magnetic moments were studied also in the quark model [17], and therefore, the present study provides one of the alterna-

tive descriptions.

Experimentally, magnetic moments of resonance states can be extracted through bremsstrahlung processes. So far, the magnetic moments of  $\Delta^{++}(1232)$  have been studied in the reaction  $\pi^+p \rightarrow \gamma\pi^+p$  [18, 19], where  $\mu_{\Delta^{++}} = 3.7 \sim 7.5\mu_N$  was extracted [20]. The uncertainty in the number arises from the ambiguity in the theoretical analysis of the reaction. Now for  $N(1535)$ , a similar process can be used such as  $\gamma p \rightarrow \gamma\eta p$  [17].

This paper is organized as follows. In section II, we present the formulation to calculate the magnetic moments in the chiral unitary model. The input parameters and numerical results are presented in section III. In section IV we discuss the obtained results from various point of view. In section V, we discuss the possibility to observe the magnetic moments of  $N^*$  in experiment and calculate the energy spectra and the angular distributions of the emitted photon in the  $\gamma N \rightarrow \gamma\eta N$  and  $\pi^-p \rightarrow \gamma\eta n$  reactions. Section VI is devoted as the summary of the present results.

## II. FORMULATION

In this section, we briefly explain the chiral unitary model, where we obtain the amplitude of meson-baryon scatterings. The amplitude of  $\pi N$  scatterings obtained in the chiral unitary model can be interpreted as the resonance pole term around the  $N(1535)$  resonance energy region, as shown in the upper diagram in Fig. 1. We then introduce the photon field and electromagnetic couplings based on effective chiral Lagrangian, and we calculate the amplitude for the photon-resonance coupling as shown in Fig. 1. Using these two amplitudes, we evaluate the magnetic moments of the resonance in two different ways. Here we follow the formulation in Ref. [16].

---

\*Present address: ECT\*, European Centre for Theoretical Studies in Nuclear Physics and Related Areas Villa Tambosi, Strada delle Tabarelle 286, I-38050 Villazzano (Trento), Italy

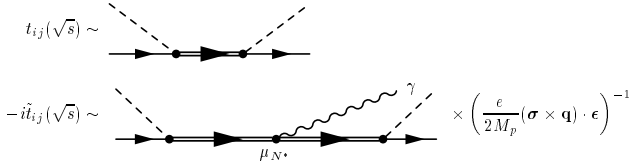


FIG. 1: Feynman diagrams of the amplitudes  $t_{ij}(\sqrt{s})$  and  $-it_{ij}(\sqrt{s})$  around energy region of the resonance. Solid, dashed, wavy and double lines represent baryons, mesons, photon and baryon resonances, respectively. In calculating  $-it_{ij}(\sqrt{s})$ , we consider the diagrams which contribute to the magnetic moments, and extract a factor in order to make the coupling of resonance to photon to be magnetic moment in units of the nuclear magneton.

### A. Chiral unitary model

Chiral unitary model is an extension of the chiral perturbation theory to the resonance energy region, by imposing the unitarity condition. Using the N/D method [21, 22] for the unitarity condition, the T-matrix amplitude can be written as

$$T = [1 - VG]^{-1}V, \quad (1)$$

with the basic interaction  $V$  and the loop function  $G$ , which are given in the following. This equation provides algebraically the solution to the Bethe-Salpeter equation.

We derive the basic interaction  $V$  from the chiral perturbation theory, which well describes low-energy hadron dynamics. For the  $J^P = 1/2^-$  baryons, the  $s$  wave scatterings are relevant, for which the basic meson-baryon interactions are given by the Weinberg-Tomozawa term. The non-relativistic form of the interaction term is then given by

$$V_{ij} = -\frac{C_{ij}}{4f_i f_j} (2\sqrt{s} - M_i - M_j) \sqrt{\frac{E_i + M_i}{2M_i}} \sqrt{\frac{E_j + M_j}{2M_j}}, \quad (2)$$

where the indices  $(i, j)$  denote the channels of meson-baryon scatterings and the coefficients  $C_{ij}$  are fixed by chiral symmetry. In this work we are interested in the  $N(1535)$  resonance, and therefore, we calculate the scattering amplitude with the strangeness  $S = 0$  and the electric charge  $Q = 0$  and  $Q = 1$ . The relevant channels and the coefficients  $C_{ij}$  are given in Table I. In Eq. (2),  $f_i$ ,  $M_i$ , and  $E_i$  are the meson decay constant, the observed baryon mass, and the energy of the baryon in the channel  $i$ , respectively.  $s$  denotes the total energy in the center of mass system.

In order to calculate the loop-integral function  $G$ , we

employ the dimensional regularization:

$$\begin{aligned} G_i(\sqrt{s}) &= i \int \frac{d^4q}{(2\pi)^4} \frac{2M_i}{(P-q)^2 - M_i^2} \frac{1}{q^2 - m_i^2} \\ &= \frac{2M_i}{(4\pi)^2} \left\{ a_i(\mu) + \ln \frac{M_i^2}{\mu^2} + \frac{m_i^2 - M_i^2 + s}{2s} \ln \frac{m_i^2}{M_i^2} \right. \\ &\quad + \frac{\bar{q}_i}{\sqrt{s}} \left[ \ln(s - (M_i^2 - m_i^2) + 2\sqrt{s}\bar{q}_i) \right. \\ &\quad + \ln(s + (M_i^2 - m_i^2) + 2\sqrt{s}\bar{q}_i) \\ &\quad - \ln(-s + (M_i^2 - m_i^2) + 2\sqrt{s}\bar{q}_i) \\ &\quad \left. \left. - \ln(-s - (M_i^2 - m_i^2) + 2\sqrt{s}\bar{q}_i) \right] \right\}, \quad (3) \end{aligned}$$

where  $m_i$  is the mass of the meson in channel  $i$ . The three-momentum of the intermediate meson  $\bar{q}_i$  is defined by

$$\bar{q}_i(\sqrt{s}) = \frac{\sqrt{(s - (M_i - m_i)^2)(s - (M_i + m_i)^2)}}{2\sqrt{s}}. \quad (4)$$

In Eq. (3),  $\mu$  and  $a_i(\mu)$  are the regularization scale and the subtraction constants, which will be taken as free parameters of this model.

Substituting Eqs. (2) and (3) into Eq. (1), we obtain the T-matrix amplitude of meson-baryon scatterings  $t_{ij}$ . The advantage of this model is that we obtain the amplitude  $t_{ij}$  in analytic form, so that it can be extended to the complex energy plane. When the subtraction constants  $a_i$  are properly fixed, the amplitude  $t_{ij}$  provides a good description for observables such as cross sections and phase shifts [13, 14, 15].

In the present model the pole of the amplitude can be calculated in the complex plane. From this pole, we extract the information of the resonance. Around the resonance region  $\sqrt{s} \sim M_{N^*}$ , the pole contribution becomes dominant, and the amplitude  $t_{ij}$  obtained in the chiral unitary approach can be interpreted as the Breit-Wigner form,

$$t_{ij}(\sqrt{s}) \sim \frac{g_i g_j}{\sqrt{s} - M_{N^*} + i\Gamma_{N^*}/2} + t_{ij}^{BG}, \quad (5)$$

where  $M_{N^*}$  and  $\Gamma_{N^*}$  are the mass and width of the resonance, respectively. Here the background term  $t_{ij}^{BG}$  is assumed to be slowly varying function of  $\sqrt{s}$ , and  $g_i$  gives the coupling strength of the resonance to the meson-baryon channel  $i$ . A diagrammatic interpretation of Eq. (5) is shown in Fig. 1 (upper diagram).

In practical calculations, we use two bases for the channels. When we calculate the scattering amplitudes, we adopt the physical basis such as  $\pi^- p$  and  $\eta n$ , because in the following subsections we introduce the electromagnetic interactions, which are not isospin symmetric. While, when we calculate the resonance properties, we change the basis to the isospin basis such as  $\pi N (I = 1/2)$

TABLE I:  $C_{ij}(S=0, Q=0)$  and  $C_{ij}(S=0, Q=1)$ 

	$C_{ij}(S=0, Q=0)$						$C_{ij}(S=0, Q=1)$						
	$\pi^0 n$	$\pi^- p$	$\eta n$	$K^0 \Lambda$	$K^0 \Sigma^0$	$K^+ \Sigma^-$	$\pi^0 p$	$\pi^+ n$	$\eta p$	$K^+ \Lambda$	$K^+ \Sigma^0$	$K^0 \Sigma^+$	
$\pi^0 n$	0	$-\sqrt{2}$	0	$\frac{\sqrt{3}}{2}$	$-\frac{1}{2}$	$-\frac{1}{\sqrt{2}}$	$\pi^0 p$	0	$\sqrt{2}$	0	$-\frac{\sqrt{3}}{2}$	$-\frac{1}{2}$	$\frac{1}{\sqrt{2}}$
$\pi^- p$		1	0	$-\sqrt{\frac{3}{2}}$	$-\frac{1}{\sqrt{2}}$	0	$\pi^+ n$		1	0	$-\sqrt{\frac{3}{2}}$	$\frac{1}{\sqrt{2}}$	0
$\eta n$			0	$-\frac{3}{2}$	$-\frac{\sqrt{3}}{2}$	$-\sqrt{\frac{3}{2}}$	$\eta p$			0	$-\frac{3}{2}$	$\frac{\sqrt{3}}{2}$	$-\sqrt{\frac{3}{2}}$
$K^0 \Lambda$				0	0	0	$K^+ \Lambda$			0	0	0	0
$K^0 \Sigma^0$					0	$-\sqrt{2}$	$K^+ \Sigma^0$				0		$\sqrt{2}$
$K^+ \Sigma^-$						1	$K^0 \Sigma^+$						1

and  $K\Sigma(I=3/2)$ , in order to specify the isospin of resonances. The two bases are related each other through the Clebsh-Gordan coefficients.

### B. Electromagnetic interactions

By gauging the baryon kinetic term in the lowest order  $\mathcal{O}(p)$  Lagrangian, we obtain the  $BB\gamma$  coupling, which provides the normal magnetic moments of the ground state baryons. In the effective chiral Lagrangian of order  $\mathcal{O}(p^2)$ , the photon coupling terms is given by [23]

$$\begin{aligned} \mathcal{L}_{(\gamma)}^{MB} = & -\frac{i}{4M_P} b_6^F \text{Tr} (\bar{B}[S^\mu, S^\nu][F_{\mu\nu}^+, B]) \\ & -\frac{i}{4M_P} b_6^D \text{Tr} (\bar{B}[S^\mu, S^\nu]\{F_{\mu\nu}^+, B\}) \end{aligned}, \quad (6)$$

where  $M_P$  is the mass of proton,  $b_6^F$  and  $b_6^D$  are the low energy constants,  $F_{\mu\nu}^+ = -e(\xi^\dagger Q F_{\mu\nu} \xi + \xi Q F_{\mu\nu} \xi^\dagger)$  with  $\xi = \exp\{i\Phi/\sqrt{2}f\}$ ,  $Q = \text{diag}(2, -1, -1)/3$  and  $S^\mu$  is a covariant baryon spin operator.  $B$  and  $\Phi$  are the octet baryon and meson fields, respectively. This Lagrangian has contributions to anomalous magnetic moments. Expanding the  $\xi$  fields, we obtain the the magnetic moments of the ground state baryons in terms of  $b_6^D$  and  $b_6^F$  in the chiral limit, which satisfy the following Coleman-Glashow relations [24];

$$\begin{aligned} \mu_{\Sigma^+} &= \mu_p, & 2\mu_\Lambda &= \mu_n, & \mu_{\Sigma^-} &= \mu_{\Xi^-}, \\ \mu_{\Xi^0} &= \mu_n, & \mu_{\Sigma^-} + \mu_n &= -\mu_p, \\ 2\mu_{\Sigma^0\Lambda} &= -\sqrt{3}\mu_n, & 2\mu_{\Sigma^0} &= \mu_{\Sigma^+} + \mu_{\Sigma^-}. \end{aligned} \quad (7)$$

Recall that the magnetic moments derived from the Lagrangian (6) are the anomalous magnetic moments, while the normal magnetic moments come from the covariant derivative. However, the contributions from the normal magnetic moments are exactly the same as the first term of Eq. (6). Indeed the normal magnetic moments just shift  $b_6^F \rightarrow b_6^F + 1$ . Therefore we will absorb the normal magnetic moments into  $b_6^F$  in the rest of this article, in order to include the normal part into  $b_6^F$  coefficients. We need to be careful that the values we show are different

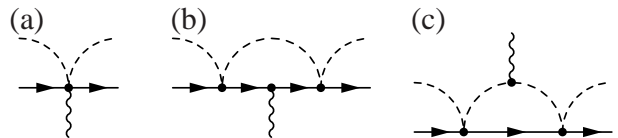


FIG. 2: Photon coupling diagram in  $-i\tilde{t}_{ij}(\sqrt{s})$ . We consider that there are meson-baryon loops on the left and right sides of these vertices.

from the low energy constant  $b_6^F$  which appears in chiral perturbation theory.

Fitting the magnetic moments written in terms of  $b_6^D$  and  $b_6^F$  to data, we find the parameters [23]

$$b_6^D = 2.39, \quad b_6^F = 1.77. \quad (8)$$

In spite of the use of the only two parameters, the tree level calculation provides good results.

### C. Photon coupling to resonances

Using the meson-baryon scattering amplitude  $t_{ij}$  obtained in the chiral unitary approach and electromagnetic couplings obtained in previous subsections, here we calculate the photon coupling diagram as shown in the bottom of Fig. 1. In the chiral unitary model, where the baryon resonances are expressed as multiple scatterings of meson-baryon states, we have three kinds of diagrams of the photon couplings as shown in Fig. 2 [16]. Among them, the diagram (c) does not contribute to the present calculation, because we consider  $s$  wave scattering. Then, we write the amplitudes  $-i\tilde{t}_{ij}(\sqrt{s})$  as

$$-i\tilde{t}_{ij}(\sqrt{s}) = \left(-i\tilde{t}_{ij}^{(a)}(\sqrt{s})\right) + \left(-i\tilde{t}_{ij}^{(b)}(\sqrt{s})\right), \quad (9)$$

where  $-i\tilde{t}_{ij}^{(a)}(\sqrt{s})$  and  $-i\tilde{t}_{ij}^{(b)}(\sqrt{s})$  are the contributions which includes the couplings of (a) and (b) in Fig. 2.

The five point (two mesons, two baryons, and one photon) vertex in Fig. 2 (a) is derived from the Lagrangian (6), by taking the terms with two mesons. We calculate the amplitude of the tree vertex (a) with these

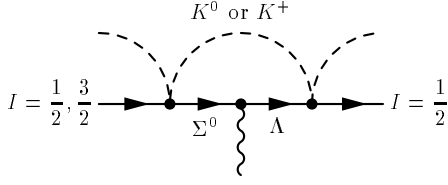


FIG. 3: Diagrams of off-diagonal components in  $\tilde{G}$  including  $\Sigma^0\Lambda$  transition in the  $S = 0$  channel.

terms as

$$V_{ij}^{BBMM\gamma} = ie \frac{\boldsymbol{\sigma} \times \mathbf{q}}{2M_p} \cdot \boldsymbol{\epsilon} A_{ij},$$

where

$$A_{ij} = \frac{1}{2f^2} [X_{ij} b_6^D + Y_{ij} b_6^F], \quad (10)$$

for convenience. Coefficients  $X_{ij}$  and  $Y_{ij}$  are shown in Tables II and III. In order to calculate the resonance magnetic moments, we attach the meson-baryon scattering amplitude obtained in the chiral unitary model to the both side of the diagram (a) in Fig. 2. We then obtain

$$-i\tilde{t}_{ij}^{(a)} = t_{il} G_l A_{lm} G_m t_{mj}. \quad (11)$$

The diagram (b) in Fig. 2 is calculated by magnetic moments of the ground state baryons  $\mu_i$  multiplying by a loop function with the two baryon propagators. In the limit that the photon momentum goes to zero, this loop function reduces to a simple form as

$$\begin{aligned} & \tilde{G}_i(\sqrt{s}) \\ &= i \int \frac{d^4 q}{(2\pi)^4} \frac{2M_i}{(P-q)^2 - M_i^2} \frac{2M_i}{(P-q)^2 - M_i^2} \frac{1}{q^2 - m_i^2} \\ &= -\frac{\partial}{\partial \sqrt{s}} G_i(\sqrt{s}). \end{aligned} \quad (12)$$

This analytic form of  $\tilde{G}_i(\sqrt{s})$  is convenient when we search the poles of the amplitude in the complex plane, which correspond to resonances. Finally we obtain

$$-i\tilde{t}_{ij}^{(b)} = t_{il} \tilde{G}_l \mu_l t_{lj}, \quad (13)$$

where  $\mu_l$  are the magnetic moments of the ground state baryons.

Since there is the  $\Sigma^0\Lambda$  transition moment in the ground state, off-diagonal components exist in  $\tilde{G}$  as shown in Fig. 3. In order to take it into account, we need further approximation, because the masses in the first and second propagators in Eq. (12) are different. We calculate these off-diagonal components by taking average of the  $\Sigma^0$  and  $\Lambda$  propagators, namely,

$$\tilde{G}_{M\Lambda, M\Sigma^0}(\sqrt{s}) = \frac{1}{2} \left( \tilde{G}_{M\Sigma^0}(\sqrt{s}) + \tilde{G}_{M\Lambda}(\sqrt{s}) \right), \quad (14)$$

where  $M$  denotes  $K^0$  or  $K^+$ . Then Eq. (13) is modified as

$$-i\tilde{t}_{ij}^{(b)} = t_{il} [\delta_{lm} \tilde{G}_l \mu_l + \tilde{G}_{l,m} \mu_{(\Sigma^0\Lambda)}] t_{mj}, \quad (15)$$

where  $\tilde{G}_{l,m} \mu_{(\Sigma^0\Lambda)}$  represents the corresponding transition channels as shown in Fig. 3.

As pointed out in Ref. [16], the effects of  $\Sigma^0\Lambda$  transition is almost negligible in the  $S = -1$  channel, where the corresponding processes are  $\pi^0\Sigma^0 \rightarrow \pi^0\Lambda$  and  $\eta\Sigma^0 \rightarrow \eta\Lambda$ . These transition terms do not contribute to the magnetic moments of  $\Lambda$  resonances ( $I = 0$ ) in the isospin limit. However, for the  $N$  resonance they do. The  $\Sigma^0\Lambda$  transition occurs among the  $K\Sigma_0$  and  $K\Lambda$  channels of  $I = 1/2$ . After projecting them to  $I = 1/2$  state, we have checked numerically that the inclusion of the  $\Sigma^0\Lambda$  transition has a moderate effect to the amplitude  $-i\tilde{t}_{ij}^{(b)}$ .

In this way, we obtain the amplitude  $-i\tilde{t}$  through Eqs. (9), (11) and (15) in the chiral unitary model. Around the resonance energy region, where the pole contribution becomes dominant,  $-i\tilde{t}$  obtained in the chiral unitary model can be interpreted using the Breit-Wigner form of resonance:

$$\begin{aligned} -i\tilde{t}_{ij}(\sqrt{s}) &\sim \left( \frac{g_i}{\sqrt{s} - M_{N^*} + i\Gamma_{N^*}/2} + t^{BG} \right) \\ &\cdot \mu_{N^*} \cdot \left( \frac{g_j}{\sqrt{s} - M_{N^*} + i\Gamma_{N^*}/2} + t^{BG} \right), \end{aligned} \quad (16)$$

where  $\mu_{N^*}$  is the magnetic moment of the  $N^*$  resonance.

#### D. Evaluation of the magnetic moments

Here we evaluate the magnetic moments of the resonances from the amplitudes  $t_{ij}$  and  $-i\tilde{t}_{ij}$  obtained by the chiral unitary model. Around the resonance energy region  $\sqrt{s} \sim M_{N^*}$ , we can regard these amplitudes as Eqs. (5) and (16), respectively. Using  $t_{ij}$ , we eliminate the resonance propagators and couplings  $g_i$  in  $-i\tilde{t}_{ij}$ . There are two methods, one is to extract them on the real axis and the other is to evaluate them in the complex plane [16].

On the real axis, in the resonance dominance, where background terms are neglected, the magnetic moment can be evaluated by

$$\mu_{N^*}(\sqrt{s}) \sim \frac{-i\tilde{t}_{ij}(\sqrt{s})}{-\frac{\partial}{\partial \sqrt{s}} t_{ij}(\sqrt{s})}, \quad (17)$$

where the denominator cancels the two resonance propagators and couplings, leaving the factor of magnetic moment. In actual cases, however, there are background contributions, which we have to deal with carefully. To show explicitly, the amplitude  $-i\tilde{t}_{ij}$  in Eq. 17 with the

TABLE II:  $X_{ij}$  and  $Y_{ij}(S=0, Q=0)$ 

	$X_{ij}$						$Y_{ij}$					
	$\pi^0 n$	$\pi^- p$	$\eta n$	$K^0 \Lambda$	$K^0 \Sigma^0$	$K^+ \Sigma^-$	$\pi^0 n$	$\pi^- p$	$\eta n$	$K^0 \Lambda$	$K^0 \Sigma^0$	$K^+ \Sigma^-$
$\pi^0 n$	0	$\frac{1}{\sqrt{2}}$	0	0	0	$\frac{1}{2\sqrt{2}}$	0	$\frac{1}{\sqrt{2}}$	0	0	0	$-\frac{1}{2\sqrt{2}}$
$\pi^- p$		-1	0	$\frac{1}{2\sqrt{6}}$	$-\frac{1}{2\sqrt{2}}$	0		-1	0	$\frac{\sqrt{6}}{4}$	$\frac{1}{2\sqrt{2}}$	0
$\eta n$			0	0	0	$\frac{\sqrt{6}}{4}$			0	0	0	$-\frac{\sqrt{6}}{4}$
$K^0 \Lambda$				0	0	$-\frac{1}{\sqrt{6}}$			0	0	0	0
$K^0 \Sigma^0$					0	0				0	0	$-\frac{1}{\sqrt{2}}$
$K^+ \Sigma^-$						-1						1

TABLE III:  $X_{ij}$  and  $Y_{ij}(S=0, Q=1)$ 

	$X_{ij}$						$Y_{ij}$					
	$\pi^0 p$	$\pi^+ n$	$\eta p$	$K^+ \Lambda$	$K^+ \Sigma^0$	$K^0 \Sigma^+$	$\pi^0 p$	$\pi^+ n$	$\eta p$	$K^+ \Lambda$	$K^+ \Sigma^0$	$K^0 \Sigma^+$
$\pi^0 p$	0	$\frac{1}{\sqrt{2}}$	0	$-\frac{1}{4\sqrt{3}}$	$\frac{1}{4}$	0	0	$\frac{1}{\sqrt{2}}$	0	$-\frac{\sqrt{3}}{4}$	$-\frac{1}{4}$	0
$\pi^+ n$		1	0	$-\frac{1}{\sqrt{6}}$	$-\frac{1}{\sqrt{2}}$	0		1	0	$-\frac{\sqrt{3}}{2}$	$\frac{1}{\sqrt{2}}$	0
$\eta p$			0	$-\frac{1}{4}$	$\frac{\sqrt{3}}{4}$	0			0	$-\frac{3}{4}$	$-\frac{\sqrt{3}}{4}$	0
$K^+ \Lambda$				1	$-\frac{1}{\sqrt{3}}$	$-\frac{1}{\sqrt{6}}$			0	0	0	0
$K^+ \Sigma^0$					-1	0				0	0	$\frac{1}{\sqrt{2}}$
$K^0 \Sigma^+$						0						0

background term included, should be divided by the factor

$$\frac{\partial}{\partial \sqrt{s}} t_{ij}(\sqrt{s}) = -\frac{g_i g_j}{(\sqrt{s} - M_{N^*} + i\Gamma_{N^*}/2)^2} + \frac{\partial}{\partial \sqrt{s}} t_{ij}^{BG}. \quad (18)$$

However, since the background term  $t_{ij}^{BG}$  is assumed to be a slowly varying function of  $\sqrt{s}$ , its derivative must be small, therefore we can neglect it. The result is

$$\begin{aligned} \frac{-i\tilde{t}_{ij}(\sqrt{s})}{-\frac{\partial}{\partial \sqrt{s}} t_{ij}(\sqrt{s})} &= \mu_{N^*}(\sqrt{s}) \\ &+ t^{BG} \frac{\sqrt{s} - z_{N^*}}{g_i} + t^{BG} \frac{\sqrt{s} - z_{N^*}}{g_j} \\ &+ (t^{BG})^2 \frac{(\sqrt{s} - z_{N^*})^2}{g_i g_j}, \end{aligned} \quad (19)$$

where  $z_{N^*} \equiv M_{N^*} - i\Gamma_{N^*}/2$ . Note that the second and third lines in Eq. (19) are not always regarded as small, because  $z_{N^*}$  has an imaginary part, so that  $(\sqrt{s} - z_{N^*})$  cannot be zero. In order to make these background terms small, we evaluate  $\mu_{N^*}$  at  $\sqrt{s} \sim M_{N^*}$  and choose the suitable channel which strongly couples to the resonance.

The analytic form of the amplitude enable us to calculate the magnetic moment in the complex plane. It is a big advantage of the chiral unitary model, since we can calculate the magnetic moment exactly on the pole and, therefore, the background terms do not give any contri-

butions. At the resonance pole  $z \rightarrow z_{N^*}$ , we calculate

$$\begin{aligned} &\lim_{z \rightarrow z_{N^*}} (z - z_R) \frac{-i\tilde{t}_{ij}(z)}{t_{ij}(z)} \\ &= \lim_{z \rightarrow z_{N^*}} \left[ \frac{\mu_{N^*}(z)}{1 + (z - z_{N^*})t^{BG}/(g_i g_j)} + \mathcal{O}(z - z_{N^*}) \right] \\ &= \mu_{N^*}(z_{N^*}). \end{aligned} \quad (20)$$

Since the position of the pole generated in the unitarization does not depend on the channel, the result (20) is independent of the channel chosen to calculate the magnetic moments.

In the second method, we can compute  $\mu_{N^*}(z_{N^*})$  without ambiguity, but with a complex phase. Because of this, we discuss only the absolute value  $|\mu_{N^*}(z_{N^*})|$ . On the other hand, in the first method, we can determine the sign, although the background terms make the absolute values ambiguous. We can minimize such ambiguities by choosing the most relevant channel, where the coupling strength of the pole  $g_i$  is the largest.

Hence, our strategy here is to calculate the absolute value in the complex plane and determine the sign on the real axis. It is not trivial that  $|\mu_{N^*}(z_R)|$  and  $|\mu_{N^*}(\sqrt{s})|$  take a same value, but we expect that they should be close each other.

### III. NUMERICAL RESULTS

In this section, we show the results of numerical calculations. First, we present the input parameters and calcu-

late  $S = 0$  meson-baryon scatterings in the chiral unitary model. Next, using the same parameters, we calculate the magnetic moments of the  $N(1535)$  resonance. In the following, we denote the two charge states of  $N(1535)$  as  $n^*(Q = 0)$  and  $p^*(Q = 1)$ .

### A. The $N(1535)$ resonance in the chiral unitary model

The resonance states are obtained by solving the scattering equation (1), whose coefficients  $C_{ij}$  are shown in Table I. The coefficients  $X_{ij}$  and  $Y_{ij}$  for the magnetic moments are given in Tables II and III. For the mass of the particles  $m_i$  and  $M_i$ , and the magnetic moments of the ground state baryons  $\mu_i$ , we use the physical values taken from the Particle Data Group (PDG) [20]. The low energy constants  $b_6^F$  and  $b_6^D$  are given by Eq. (8). In order to calculate the loop function (3), we use the regularization scale  $\mu = 630$  MeV and the following channel dependent subtraction constants taken from Ref. [13];

$$\begin{aligned} a_{\pi N} &= 0.711, & a_{\eta N} &= -1.09, \\ a_{K\Lambda} &= 0.311, & a_{K\Sigma} &= -4.09. \end{aligned} \quad (21)$$

Here we show the shifted values of  $a_i$  corresponding to  $\mu = 630$  MeV by using the relation  $a(\mu') = a(\mu) + 2\ln(\mu'/\mu)$ . We use the common value for each isospin multiplet. These constants are essential to generate the  $N(1535)$  resonance [25, 26]. We adopt the physical meson decay constants,

$$f_\pi = 93 \text{ [MeV]}, \quad f_K = 1.22 \times f_\pi, \quad f_\eta = 1.3 \times f_\pi, \quad (22)$$

following Ref. [13].

Using these inputs, we calculate the scattering amplitudes (1), which well describes the  $S_{11}$  phase shifts, the scattering amplitudes and the total cross section of  $\pi^- p \rightarrow \eta n$ . In the complex energy plane, we find poles at

$$\begin{aligned} z_{n^*} &= 1536.01 - 37.06i \text{ [MeV]} \quad (Q = 0), \\ z_{p^*} &= 1531.01 - 36.38i \text{ [MeV]} \quad (Q = 1), \end{aligned} \quad (23)$$

whose real and imaginary parts correspond to the mass  $M_{N^*}$  and width  $\Gamma_{N^*}/2$ , respectively, for the Breit-Wigner parametrization (5). Note that before including the electromagnetic interactions, the difference between  $n^*$  and  $p^*$  comes from the tiny isospin violation due to the particle mass differences. Their coupling strengths  $|g_i|^2$  to the various meson-baryon channels are shown in Table IV. From this table, we see that the  $K\Sigma$  channel has the largest coupling strength to the  $N(1535)$  resonance, which indicates that the resonance is a quasi-bound state of  $K\Sigma$ , as pointed out in Ref. [7]. At the energy of the threshold of  $N(1535)$ , the  $\pi N$  and  $\eta N$  channels open. Therefore, the decay of the resonance is dominated by  $\eta N$  channel, which is a characteristic properties of  $N(1535)$ .

TABLE IV: Coupling strengths of the  $N(1535)$  resonance to meson-baryon channels. All the channels have isospin  $I = 1/2$ .

	$ g_{\pi N} ^2$	$ g_{\eta N} ^2$	$ g_{K\Lambda} ^2$	$ g_{K\Sigma} ^2$
$n^*$	0.623	2.30	1.93	7.29
$p^*$	0.619	2.35	1.88	7.37

### B. Magnetic moments of the $N(1535)$ resonance

We first show the results in the complex plane, calculated from Eq. (20). The results for the absolute values are

$$|\mu_{n^*}| = 0.248\mu_N, \quad |\mu_{p^*}| = 1.13\mu_N. \quad (24)$$

As expected, we have checked that the results are channel independent, since we can eliminate the background contributions.

Next we calculate  $\mu(\sqrt{s})$  on the real axis. In Fig. 4, we plot the scattering amplitudes  $N = -i\tilde{t}_{ij}(\sqrt{s})$  and  $D = -\frac{\partial}{\partial\sqrt{s}}t_{ij}(\sqrt{s})$ , and the magnetic moments  $\mu \sim N/D$ . Here we plot the amplitudes  $K\Sigma \rightarrow K\Sigma(I = 1/2)$ , since it has the largest coupling strength to the resonance and background contributions are expected to be small. Notice that the amplitudes  $D$  do not contain the electromagnetic interaction, and therefore,  $D$  for  $Q = 0$  and  $Q = 1$  are the same when isospin violation is neglected. On the other hand, the amplitudes  $N$  are different from each other due to the photon couplings. It is important that  $N(Q = 0)$  and  $N(Q = 1)$  have opposite signs. These signs together with  $D$  determines the sign of the magnetic moments.

If there were no background, for both  $N$  and  $D$ , extreme values of the real parts and zeros of the imaginary parts would have taken place at the same value  $\sqrt{s} = M_{N^*}$ . In this case,  $\mu = N/D$  becomes pure real. However, in actual calculations these points deviate slightly, especially in  $Q = 0$ , due to background contributions. Therefore, we evaluate the magnetic moments at all these points. Since  $\mu = N/D$  has a small imaginary part due to the backgrounds, we calculate  $\mu$  as,

$$\mu = \text{Re} \left[ \frac{-i\tilde{t}_{ij}(\sqrt{s})}{-\frac{\partial}{\partial\sqrt{s}}t_{ij}(\sqrt{s})} \right]. \quad (25)$$

The results are shown in the bottom figures of Fig. 4. Then we determine the value of the magnetic moments of the resonance

$$\begin{aligned} \mu_{n^*} &= (-0.266 \pm 0.01)\mu_N, \\ \mu_{p^*} &= (1.26 \pm 0.02)\mu_N, \end{aligned} \quad (26)$$

with small uncertainties. The absolute values of Eq. (26) do not differ very much from the results (24). This is because we adopt the  $K\Sigma$  channel, where  $|g_i|^2$  is the largest.

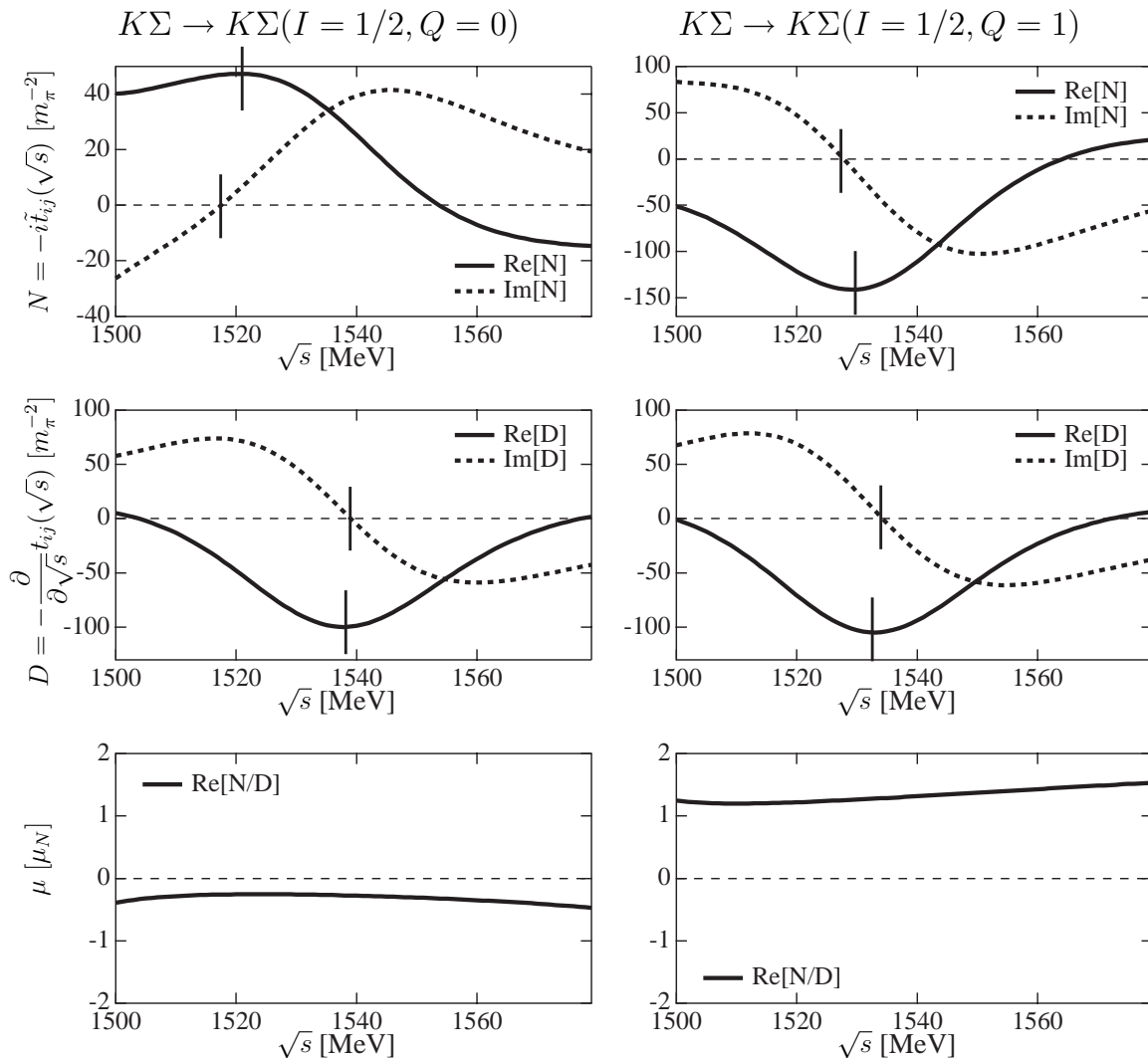


FIG. 4: Scattering amplitudes and the magnetic moments on the real axis. We plot the real and imaginary parts of the  $K\Sigma \rightarrow K\Sigma$  amplitudes  $N = -it_{ij}(\sqrt{s})$  and  $D = -\frac{\partial}{\partial\sqrt{s}}t_{ij}(\sqrt{s})$ , in  $Q = 0$  and  $Q = 1$ . Solid bars represent the position  $\sqrt{s} = M_R$ , expected by the Breit-Wigner form. The magnetic moments  $\mu = \text{Re}[N/D]$  are calculated in units of the nuclear magneton.

When we choose the other channels to evaluate the magnetic moments, the difference from the results (24) becomes larger, due to the background effects (second and third lines of Eq. (19)).

Finally we summarize the results in Table V. Combining the results in the complex plane and on the

TABLE V: The magnetic moments of the  $N(1535)$  resonance in units of the nuclear magneton.

	$n^*$	$p^*$
$ \mu $ (complex plane)	0.248	1.13
$\mu$ (real axis)	$-0.266 \pm 0.01$	$1.26 \pm 0.02$

real axis, we determine the magnetic moments as

$$\mu_{n^*(1535)} = -0.25\mu_N, \quad \mu_{p^*(1535)} = 1.1\mu_N. \quad (27)$$

In next section, we discuss these results in detail.

#### IV. DISCUSSIONS

First we discuss the SU(3) relation by comparing the present results with the magnetic moment of  $\Lambda(1670)$  obtained in the same framework [16]. Then we decompose the magnetic moment into the various components in order to understand the origin of the obtained values. Then we discuss the magnetic moments in the quark model and chiral doublet model, in comparison with the present results.

TABLE VI: Coupling strengths  $|g_i|^2$  of  $N(1535)$  and  $\Lambda(1670)$  in SU(3) basis. Values for  $\Lambda^*(1670)$  are taken from Ref. [27]

representation	1	8	8	10	$\bar{10}$	27
$n^*(1535)$	–	5.2	6.2	0.17	–	0.58
$\Lambda^*(1670)$	4.0	2.3	7.3	–	–	0.16

### A. The SU(3) relation

In Ref. [16], the magnetic moments of  $\Lambda(1670)$  are calculated in the chiral unitary model;

$$\mu_{\Lambda^*(1670)} = -0.29\mu_N . \quad (28)$$

The  $\Lambda(1670)$  and  $N(1535)$  have  $J^P = 1/2^-$ , so that they have been considered to be members of the SU(3) octet. If the SU(3) symmetry is exact, the magnetic moments of the octet should satisfy the Coleman-Glashow relations in Eq. (7), which tell us that

$$\mu_{n^*} = 2\mu_{\Lambda^*} . \quad (29)$$

In the present calculation, the signs of the magnetic moments in Eqs. (26) and (28) are consistent with this relation, although the absolute values do not agree with Eq. (29).

The SU(3) relation is discussed more clearly by looking at the SU(3) decomposition of the resonance states in terms of the coupling strengths  $g_i$ . The coupling strengths in the SU(3) basis are obtained by a unitary transformation using SU(3) Clebsh-Gordan coefficients [27]. In Table VI,  $|g_i|^2$  in SU(3) basis are shown, where we observe that for both  $N(1535)$  and  $\Lambda(1670)$ , octet component are dominant. This fact explains qualitative agreement of the relation between  $\mu_{n^*}$  and  $\mu_{\Lambda^*}$  in the chiral unitary model. Deviation from the relation comes from the large mixture of the singlet component in  $\Lambda(1670)$  and SU(3) breaking effects.

### B. Isospin decomposition

For later discussions, we decompose the magnetic moments in Eq. (27) into isoscalar ( $\mu_S$ ) and isovector ( $\mu_V$ ) components. These moments are defined by

$$\mu_V^S = \frac{1}{2}(\mu_p \pm \mu_n) . \quad (30)$$

In units of nuclear magneton  $\mu_N = e/2M_N$ , these values are

$$\mu_S = 0.44\mu_N , \quad \mu_V = 0.69\mu_N , \quad (31)$$

The isoscalar magnetic moment of  $N(1535)$  is similar to that of the ground state nucleon  $N(939)$ , but the isovector one is much smaller than that of the nucleon  $\mu_V(939) = 2.35\mu_N$ .

More quantitatively, it is considered to express these values in units of resonance magneton  $\mu_{N^*} \equiv e/2M_{N^*}$  and extract the anomalous magnetic moments  $\kappa$  in units of  $\mu_{N^*}$ . The results are

$$\mu_S(1535) = 0.72\mu_{N^*} , \quad \mu_V(1535) = 1.13\mu_{N^*} , \quad (32)$$

and

$$\kappa_S(1535) = 0.22\mu_{N^*} , \quad \kappa_V(1535) = 0.63\mu_{N^*} . \quad (33)$$

These numbers may be compared with those of the nucleon (in units of nuclear magneton):

$$\kappa_S(939) = -0.06\mu_N , \quad \kappa_V(939) = 1.85\mu_N . \quad (34)$$

Hence the strong isovector dominance as in the  $N(939)$  magnetic moments is not realized in  $N(1535)$ .

### C. Contributions from various terms

In this subsection, we decompose the magnetic moments into various terms in order to understand qualitatively their origins. First we decompose the amplitude into the contributions from the term in Fig. 2 (a) (contact vertex) and those from in Fig. 2 (b) (photon attached to baryon propagator). We perform this decomposition for the results obtained on the real axis. In Fig. 5, we show the corresponding amplitudes for  $Q = 0$  and  $Q = 1$ . We see that the contribution from (a) is smaller in magnitude than (b), and that the contributions of (a) and (b) have opposite (same) signs for  $Q = 0$  ( $Q = 1$ ). Therefore, there is a cancellation between them for  $Q = 0$  in the total value, while for  $Q = 1$  two terms are added with the same sign. This explains partly smaller magnetic moments of  $Q = 0$  than that of  $Q = 1$ . The actual numbers around resonance region are given as

$$\begin{aligned} \mu_{n^*}^{(a)} &\sim 0.34\mu_N , & \mu_{n^*}^{(b)} &\sim -0.60\mu_N , \\ \mu_{p^*}^{(a)} &\sim 0.40\mu_N , & \mu_{p^*}^{(b)} &\sim 0.87\mu_N , \end{aligned} \quad (35)$$

where  $\mu_{n^*,p^*} = \mu_{n^*,p^*}^{(a)} + \mu_{n^*,p^*}^{(b)}$ . As compared with Eq. (31), these numbers imply that the term  $\mu^{(a)}$  is dominated by the isoscalar piece, while the term  $\mu^{(b)}$  by the isovector piece. The negligible values of  $\mu^{(a)}$  is the origin to weaken isovector dominance of the  $N(1535)$  magnetic moments.

Let us now consider the the piece  $\mu^{(b)}$  and its isovector dominance. As shown in Fig. 2 (b),  $\mu^{(b)}$  is given by a sum of the diagrams where the photon couples to a ground state baryon. In this case, we can draw a naive picture where the resonance magnetic moment can be written as a sum of the magnetic moments of the ground state baryons weighted by their probabilities in the resonance wave function. In Ref [17], considering  $N(1535)$  as a quasi-bound state of  $K\Sigma$ , they decomposed the  $K\Sigma$  isospin state into physical states by the Clebsh-Gordan



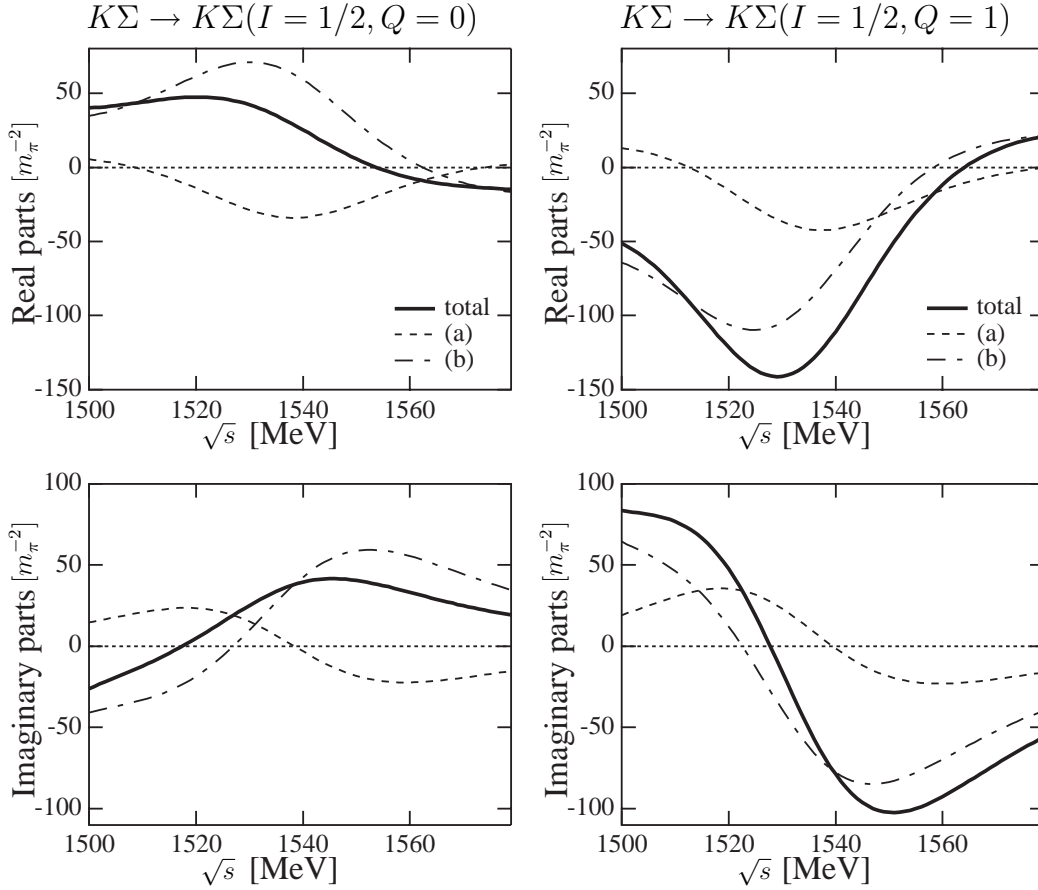


FIG. 5: Real and imaginary parts of the  $K\Sigma \rightarrow K\Sigma$  amplitudes  $-i\tilde{t}_{ij}^{(a)}$ ,  $-i\tilde{t}_{ij}^{(b)}$  and  $-i\tilde{t}_{ij} = -i\tilde{t}_{ij}^{(a)} - i\tilde{t}_{ij}^{(b)}$  (dashed, dash-dotted and solid lines) in  $Q = 0$  and  $Q = 1$ .

coefficients, and evaluate the magnetic moments of the ground state baryon. Here we extend this estimation to sum up all the channels, multiplying  $|g_i|^2$  as weight. First, we define the magnetic moments of the isospin states, using the Clebsh-Gordan coefficients and the magnetic moments of the ground states;

$$\begin{aligned}
 \mu_{\pi N}(Q=0) &= \frac{1}{3}\mu_n + \frac{2}{3}\mu_p \sim 1.22\mu_N, \\
 \mu_{\eta N}(Q=0) &= \mu_n \sim -1.91\mu_N, \\
 \mu_{K\Lambda}(Q=0) &= \mu_\Lambda \sim -0.613\mu_N, \\
 \mu_{K\Sigma}(Q=0) &= \frac{1}{3}\mu_{\Sigma^0} + \frac{2}{3}\mu_{\Sigma^-} \sim -0.557\mu_N, \\
 \mu_{\pi N}(Q=1) &= \frac{2}{3}\mu_n + \frac{1}{3}\mu_p \sim -0.343\mu_N, \\
 \mu_{\eta N}(Q=1) &= \mu_p \sim 2.79\mu_N, \\
 \mu_{K\Lambda}(Q=1) &= \mu_\Lambda \sim -0.613\mu_N, \\
 \mu_{K\Sigma}(Q=1) &= \frac{1}{3}\mu_{\Sigma^0} + \frac{2}{3}\mu_{\Sigma^+} \sim 1.86\mu_N.
 \end{aligned} \tag{36}$$

Multiplying the weight  $|g_i|^2$  in Table IV, we calculate

$$\begin{aligned}
 \mu_{n^*} &= \frac{|g_{\pi N}|^2}{\sum_j |g_j|^2} \mu_{\pi N} + \frac{|g_{\eta N}|^2}{\sum_j |g_j|^2} \mu_{\eta N} \\
 &\quad + \frac{|g_{K\Lambda}|^2}{\sum_j |g_j|^2} \mu_{K\Lambda} + \frac{|g_{K\Sigma}|^2}{\sum_j |g_j|^2} \mu_{K\Sigma}.
 \end{aligned} \tag{37}$$

The results are

$$\mu_{n^*} \sim -0.74\mu_N, \quad \mu_{p^*} \sim 1.55\mu_N, \tag{38}$$

which are similar values with those obtained in Ref. [17] ( $\mu_{n^*} \sim -0.56\mu_N$  and  $\mu_{p^*} \sim 1.86\mu_N$ ), because in Eq. (37) the  $K\Sigma$  component ( $|g_{K\Sigma}|^2$ ) dominates the  $N(1535)$  resonance ( $\sim 60\%$ ). Naively, it is expected that this estimation corresponds to the contribution from  $-i\tilde{t}_{ij}^{(b)}$ , where the magnetic moments of the ground states are summed.

#### D. Comparison with quark model

Here we discuss the present results in comparison with the quark model results. The details how to compute the resonance magnetic moments have been presented

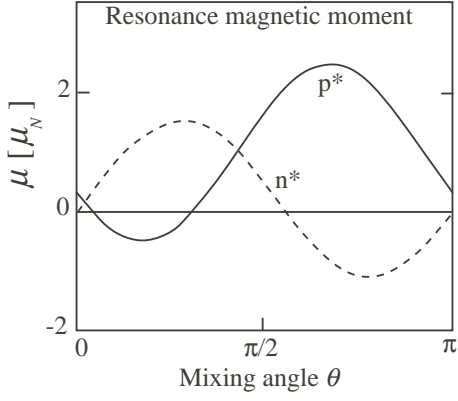


FIG. 6: Magnetic moments as a function of the mixing angle  $\theta$  in units of the nuclear magneton.

previously [17], and therefore, here we show some relevant points. In the quark model, the wave function of  $N(1535)$  is given as a superposition of two spin ( $s = 1/2$  and  $3/2$ ) states in the  $l = 1$  70-dimensional representation of  $SU(6)$ :

$$|N(1535)\rangle = \cos\theta|s = 1/2\rangle + \sin\theta|s = 3/2\rangle, \quad (39)$$

where  $\theta$  is a mixing angle of the two states. Actually, the spin  $s = 1/2, 3/2$  states are coupled with the orbital angular momentum  $l = 1$  to yield  $j = s + l = 1/2$ . The magnetic moment operator is a sum of spin and orbital angular momenta of three quarks,

$$\mu = \frac{1}{2m} \sum_{i=1,2,3} (\sigma_3(i) + l_3(i)). \quad (40)$$

By taking a matrix element between the quark model state (39), we obtain the magnetic moment as a function of the mixing angle  $\theta$ .

The result is presented in Fig. 6. As reported in Ref. [17], the mixing angle  $\theta \sim 150 \sim -30$  degrees of the Isgur-Karl quark model yields the values

$$\mu_{n^*} = -1.2\mu_N, \quad \mu_{p^*} = 1.9\mu_N. \quad (41)$$

Although these numbers differ quantitatively from those in the chiral unitary model, they look similar qualitatively. In fact, it is interesting to observe that this happens only in the vicinity of the mixing angle  $\theta \sim 150$  degree. The similarity between the predictions in the quark model and the chiral unitary model was also reported for the axial coupling constant of  $N^*$ , or equivalently the  $\pi N^* N^*$  coupling constant (due to the Goldberger-Treiman relation) [28].

### E. Magnetic moments in the chiral doublet model

In this section, we present yet another description for magnetic moments when the resonance of negative parity is regarded as a chiral partner of the ground state

nucleon in linear representations of chiral symmetry. In addition to phenomenological aspects, such a point of view may shed a light on the properties of spontaneous breaking of chiral symmetry. The theoretical scheme for positive and negative parity nucleons has been discussed in detail in Ref. [4, 6], and here we follow the essence of their description. The relevant point is that the chirality structure of the electromagnetic coupling; the vector coupling is of chirality even, while the tensor (anomalous magnetic) coupling is of chirality odd:

$$\begin{aligned} \mathcal{L}_{\gamma NN} &= \bar{N} \left( \gamma_\mu + i\kappa_\alpha \frac{\sigma_{\mu\nu} q^\nu}{2M_P} \right) \tau_\alpha N A^\mu \\ &= (\bar{N}_l \gamma_\mu \tau_\alpha N_l + \bar{N}_r \gamma_\mu \tau_\alpha N_r) A^\mu \\ &\quad + i\kappa_\alpha \left( \bar{N}_l \frac{\sigma_{\mu\nu} q_\nu}{2M_P} \tau_\alpha N_r + \bar{N}_r \frac{\sigma_{\mu\nu} q_\nu}{2M_P} \tau_\alpha N_l \right) A^\mu. \end{aligned} \quad (42)$$

Here  $\alpha = 0$  or  $3$ ;  $\tau_0 = 1$  is for the isoscalar and  $\tau_3$  for the isovector components of the current. The proton mass  $M_P$  is just used for the unit. The right and left handed components of the nucleon is defined by  $N_{r,l} = \frac{1 \pm \gamma_5}{2} N$ .

In the spirit of the theory of chiral symmetry, the electromagnetic coupling is regarded as a part of the chiral invariant coupling with right and left chiral fields. In Eq. (42) the vector term preserves chiral symmetry, while the tensor (anomalous) term does not appear so. In order for the latter to be chirally symmetric, it should contain the chiral field  $U_5 = \sigma + i\vec{\tau} \cdot \vec{\pi} \gamma_5$ . When chiral symmetry is broken spontaneously,  $\sigma$  takes a finite expectation value  $\langle \sigma \rangle$ , which survives the tensor term.

Another interesting possibility is to construct a chiral invariant tensor term in the mirror model for positive and negative parity nucleons [4, 6], where the basis of the chiral symmetry does not coincide to the physical basis. Denoting the two chiral basis fields as  $N_1$  and  $N_2$ , the tensor coupling term takes on the form

$$\mathcal{L}_{\gamma NN} = \frac{i\kappa}{2M_P} (\bar{N}_1 \sigma_{\mu\nu} \gamma_5 N_2 + \bar{N}_2 \sigma_{\mu\nu} \gamma_5 N_1) q^\nu A^\mu. \quad (43)$$

This is the lagrangian to the lowest order ( $n = 0$ ) in powers of  $\langle \sigma \rangle^n$  and is becoming a dominant term as chiral symmetry is getting restored,  $\langle \sigma \rangle \rightarrow 0$ . Note again that the proton mass  $M_P$  here is introduced only for the unit and has nothing to do with the dynamical generated mass of nucleon in the linear sigma model. In the following discussion, we consider only this leading order term of  $\mathcal{O}(\langle \sigma \rangle^0)$ , in order to reduce the number of free parameters.

As discussed in Ref. [4, 6], the physical nucleon and  $N(1535)$  fields are linear combinations of  $N_1$  and  $N_2$ ;  $N(939) = \cos\theta N_1 + \gamma_5 \sin\theta N_2$ ,  $N(1535) = -\gamma_5 \sin\theta N_1 + \cos\theta N_2$ , where  $\theta$  is a mixing angle. After diagonalization, the coupling term takes on the form ( $N_+ \equiv N(939)$ ,  $N_- \equiv N(1535)$ ):

$$\begin{aligned} \mathcal{L}_{\gamma NN} &= \frac{i}{2M_P} (\sin 2\theta (\bar{N}_+ \Gamma N_+ + \bar{N}_- \Gamma N_-) \\ &\quad - \cos 2\theta (\bar{N}_+ \Gamma_5 N_- + \bar{N}_- \Gamma_5 N_+)) , \end{aligned} \quad (44)$$

where we have introduced the notation  $\Gamma = \sigma_{\mu\nu}q^\nu(\kappa_S + \kappa_V\tau_3)A^\mu$ ,  $\Gamma_5 = \Gamma\gamma_5$  with  $\kappa_S$  and  $\kappa_V$  being the isoscalar and isovector contributions to the anomalous magnetic moments. We find that the anomalous magnetic moments of  $N(939)$  and  $N(1535)$  are the same;  $\kappa_p = \kappa_{p^*}$ ,  $\kappa_n = \kappa_{n^*}$ . In the chiral unitary model, however, this is not the case.

Let us now briefly discuss the transition moments. Note that the transition term has the structure of  $E1$  because of the parity. From the pion coupling strength of  $N(1535)$  decay, the mixing angle was estimated as  $\theta \sim 6.3$  degree [4, 5, 6]. We can then use the diagonal components of the magnetic moments for the proton and neutron to fix the  $\kappa$ 's:  $\kappa_S \sin 2\theta = -0.06$  and  $\kappa_V \sin 2\theta = 1.85$ . Using these numbers, we find for the transition moments:  $\mu_{pp^*} = 8.42$  and  $\mu_{nn^*} = -8.99$ . The isovector dominance in these quantities is consistent with what is known from experiment, but the magnitudes of these numbers are too large as compared with experimental data,  $|\mu_{pp^*}| \sim 2|\mu_{nn^*}| \sim 1$  in units of the nuclear magneton, as extracted from the helicity amplitudes  $A_{1/2}^{p,n} \sim 90, -46 \cdot 10^{-3} \text{GeV}^{-1/2}$  [20].

Phenomenologically, both diagonal and transition moments do not agree with data. In particular, the small mixing angle has led to the dominance of the off-diagonal components, which should be so in the world where chiral symmetry breaking is not so strong. We can make some speculations about the nature of the breaking of chiral symmetry. For instance, the fact that  $\mu_N \neq \mu_{N^*}$  could be an indication that higher order terms in  $\langle\sigma\rangle$  should be important. The large transition moments may suggest a larger mixing angle, as opposed to the result obtained from the pion couplings previously [4, 5, 6]. Both facts may be an indication that chiral symmetry is broken rather strongly. In any event, magnetic moments of the nucleon as well as of its excited state provide useful information of chiral symmetry of baryons.

## V. OBSERVATION OF THE $N^*$ MAGNETIC MOMENT

In this section, we would like to discuss possibilities of the experimental observations of the  $N^*$  magnetic moments. The  $N(1535)$  has the special feature that this resonance strongly couples to the  $\eta N$  system, which is not seen in the other  $N^*$  resonances. Thus the  $\eta$  meson in the final state may be regarded as a probe of  $N(1535)$  in the intermediate state. In order to observe the  $N(1535)$  magnetic moments, here we would like to calculate cross sections of the following two photon-emission processes;  $\gamma N \rightarrow \gamma\eta N$  and  $\pi^- p \rightarrow \gamma\eta n$ , and we investigate sensitivity of their cross sections to the value of the magnetic moments of  $N^*$ . Such processes that two-boson emission on nucleon target are discussed in Ref. [4, 29] to observe the sign of the  $\pi N^* N^*$  coupling. In the present work, we follow their method to calculate the cross sections of the above processes.

In the calculations of the cross sections, we use the Lagrangian formulation for  $N^*$ , where the  $N^*$  is described as a well-defined field and its propagator is assumed to be the Breit-Wigner form with the mass  $m_{N^*} = 1535$  MeV and the width  $\Gamma_{N^*} = 150$  MeV. The Lagrangians used in the present calculations are shown in Appendix A.

Now we assume the  $N^*$  dominance hypothesis in the  $\eta$ - $N$  system near the threshold region, that is, the  $\eta$  meson can couple only to the  $N$  and  $N^*$  transition, and the other resonances do not couple to the  $\eta$  meson. It is shown in Ref. [4] that this hypothesis reproduce the  $N(1535)$  resonance well in the  $\pi N \rightarrow \eta N$  process. Then the relevant diagrams for these processes are shown in the Fig. 7. The diagrams  $a$  and  $b$  are used only for the pion-induced process. Since we consider the photon-eta production processes in the energies close to the threshold, the final photon and eta meson have small energies and, therefore, the dominant contributions come from the diagrams  $a$ , 1, 2, 9 as a result of their small energy denominators. The diagram 2 is the one in which the magnetic moment of  $N^*$  appears, and we want to see the interference effects of this diagram with the other dominant diagrams to study the  $N^*$  magnetic moments.

The differential cross section is given as

$$d\sigma = \frac{2m_N}{4\sqrt{(p_i \cdot k_i)^2 - m_N^2 m_{IB}^2}} \frac{1}{2} \frac{1}{2} \sum_{\text{spin pol.}} |\mathcal{T}_{fi}|^2 d\Phi, \quad (45)$$

where the summation is taken over the spin of the initial and final nucleons and the polarization of the final (and initial) photon, and the factors in front of the summation are for taking averages of the spin and polarization in the final state. The mass  $m_{IB}$  denotes the mass of the initial boson, photon or pion in the present case. The phase space of the three-particle state is given by

$$d\Phi = (2\pi)^4 \delta(p_i + k_i - p_f - k_\gamma - k_\eta) \times \frac{d^3 \vec{k}_\gamma}{(2\pi)^3 2E_\pi} \frac{d^3 \vec{k}_\eta}{(2\pi)^3 2E_\eta} \frac{m_N d^3 \vec{p}_f}{(2\pi)^3 2E_f}, \quad (46)$$

where  $k_\gamma = (E_\gamma, \vec{k}_\gamma)$ ,  $k_\eta = (E_\eta, \vec{k}_\eta)$  and  $p_f = (E_f, \vec{p}_f)$  are momenta for the final photon, eta and nucleon, respectively. In the center of mass frame, Eq. (46) is written as

$$d\Phi = \frac{m_N}{4(2\pi)^5} dE_\gamma dE_f d\alpha d(\cos\beta) d\gamma. \quad (47)$$

Here  $\alpha, \beta, \gamma$  are the Euler angles, which specify the plane where the three momenta in the final state lie. The normalizations of the state and wave function for nucleon are

$$\bar{u}^{(\alpha)}(p) u^{(\beta)}(p) = \delta^{\alpha\beta}, \quad (48)$$

$$\langle p|p' \rangle = \frac{E}{m_N} (2\pi)^3 \delta^3(\vec{p} - \vec{p}'). \quad (49)$$

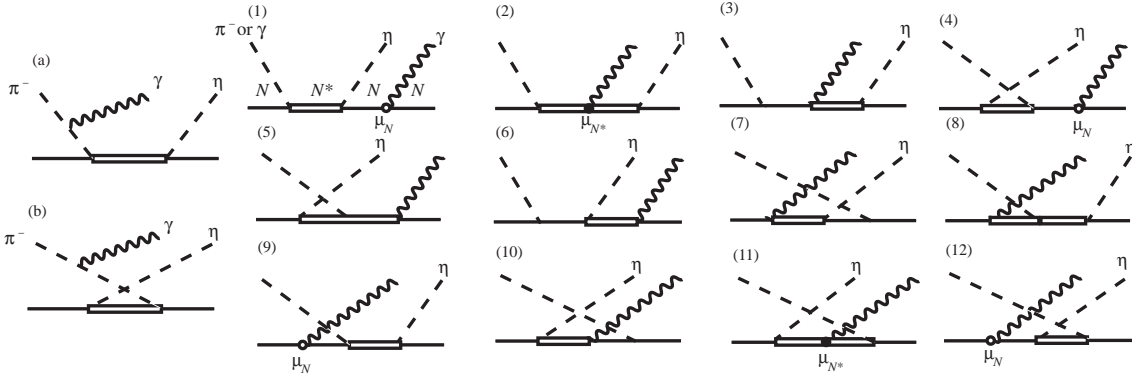


FIG. 7: The relevant diagrams for the processes  $\gamma N \rightarrow \gamma \eta N$  and  $\pi^- p \rightarrow \gamma \eta n$ . The diagram 0 is only for the pion induced process. The initial boson is either photon or pion. The solid and double-solid lines denote  $N$  and  $N^*$ , respectively. The dotted and wavy lines in the final state are the emitted photon and eta meson, respectively.

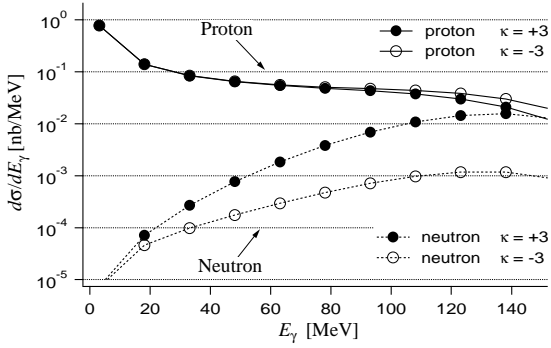


FIG. 8: Energy spectra of the emitted photon in the photon-induced process. The energy of the initial photon is 1000 MeV. The solid and dotted lines denote the proton and neutron targets, respectively. The anomalous magnetic moments of  $p^*$  and  $n^*$  are assumed to  $+3$  (black circle) or  $-3$  (white circle) in units of nuclear magneton.

In the calculations of the cross sections, we perform the integral over the three-body phase space with the Monte Carlo method. The number of the integration points in the present calculations are taken larger than 10,000, which may be enough to converge the Monte Carlo integral. The details of the Monte Carlo method for the three-body final state are discussed in Ref. [4].

Shown in Fig. 8 are the energy spectra of the emitted photon in the photon-induced processes with the proton and neutron targets;  $\gamma N \rightarrow \gamma \eta N$ . In order to see the sensitivity of the effect of the magnetic couplings of  $N^*$  to the cross sections, the anomalous magnetic moments for the nucleon resonances are assumed to be  $+3$  or  $-3$  in units of nuclear magneton, although the predicted values by the present work are much smaller.

In the case of the proton target, where we investigate the magnetic moment of  $p^*$ , the resonance magnetic moment is not sensitive to the energy spectrum of the emitted photon, as shown in Fig. 8. Presenting the sep-

arated contribution from the diagram 2, in which the  $N^*$  magnetic moment is involved, we show in Fig. 9 the energy spectra calculated with each dominant diagram of Fig. 7. In Fig. 9, it is seen that the energy spectrum for the proton target case is dominated by the contribution from the diagram 9 in all energies, which corresponds to the bremsstrahlung of the initial proton. In the bremsstrahlung, the cross section becomes larger with the faster charged particle and the softer emitted photon. The diagram 2 gives much smaller contribution than the diagram 9. Therefore the  $\gamma p \rightarrow \gamma \eta p$  is not appropriate process to observe the  $N^*$  magnetic moment. In fact, in the case of the charged particle proton, the electric coupling of the proton to the photon gives larger contributions than the magnetic one, since the magnetic coupling linearly depends on the photon momentum and, hence, is suppressed in energies near the threshold.

On the other hand, in the case of the neutron target, the sensitivity of the magnetic moment is seen in the higher energies of the spectra as a result of the interference effects. Here we would have chance to observe the magnetic moment of  $n^*$ , although the cross sections are quite small and the all participants in this reaction are neutral particles. As shown in Fig. 9, the diagram 9 is less dominant than the proton target case, since there are no electric couplings for the neutron target case. Rather than the amount of the cross section, however, distinct signals of the dependence of the magnetic moments of  $N^*$ , such as position of peak, are not seen in the energy spectra of the emitted photon.

Next we calculate the angular distributions of the emitted photon, which is expected to be a better example to see the interference effects. Shown in Fig. 10 are the calculated angular distributions in terms of the angle  $\theta$  between the incident and final photons. Here we find the distinct angular dependences in the case of the neutron target, which would be observed. We also plot in Fig. 10(b) the angular distributions with the  $N^*$  magnetic moments obtained by the chiral unitary model and the quark model. It might be difficult, however, to distin-

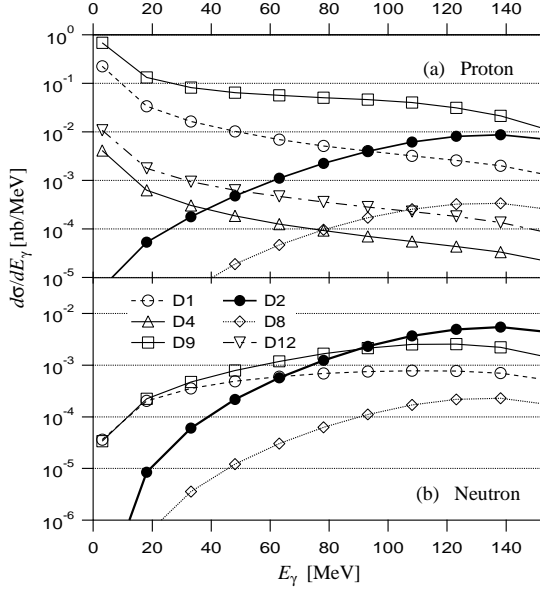


FIG. 9: Separated contributions for the dominant diagrams to the energy spectra in the photon-induced process with the initial photon energy  $E_i = 1000$  MeV. The upper panel (a) is for the proton target case. The lower panel (b) is the same for the neutron target case. The anomalous magnetic moments of  $p^*$  and  $n^*$  are  $+3\mu_N$ . The lines with black circles, open circles, triangles, diamonds, squares and down-triangles denote the contributions from the diagrams 1, 2, 4, 8, 9 and 12, respectively.

guish these two model in experiment. In the calculations of the angular distributions, we perform the integration with respect to the final photon energy from 80 MeV, since we want to see the interference effects of the diagram 2 to the others and the diagram 2 gives dominant contributions at photon energies larger than 80 MeV as seen in Fig. 9. We show in Fig. 11 the separated contributions to the angular distributions to the emitted photon. As seen in the figure, the diagram 2 becomes the dominant diagram in the case of the neutron target, while, in the proton target case, the diagram 9 is still the most dominant diagram.

Finally we discuss the pion-induced process briefly. As discussed before, in the case of neutron, the value of the  $n^*$  magnetic moment is sensitive to the cross sections, since the magnetic contributions is relatively enhanced due to the absence of the electric coupling. Thus, we would expect that the  $\pi^- p \rightarrow \gamma \eta n$  process would be good to observe the magnetic moment of  $n^*$ . Unlike our expectation, however, in this case, we conclude that it is very difficult to extract the magnetic moments of  $N^*$ , since the diagrams  $a$  and 9 are the most dominant contributions to the cross sections, as shown in Fig. 12. These diagrams corresponds to the bremsstrahlung of the initial charged particles. Since the initial pion and proton have large momenta to create the eta meson at the final state,

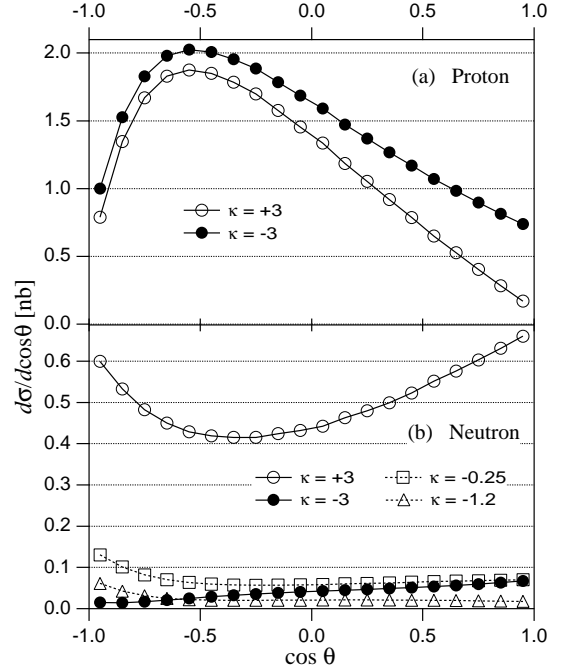


FIG. 10: Angular distributions of the emitted photon in the photo-induced process with the initial photon energy 1000 MeV. The integration with respect to the emitted energy is performed from 80 MeV to the threshold. The upper panel (a) is for the proton target, and the lower panel (b) is the same for the neutron target. The anomalous magnetic moments of  $N^*$  is assumed to  $+3$  (open circle) or  $-3$  (black circle) in units of nuclear magneton. In the case of the neutron target, the plots with the  $N^*$  magnetic moments obtained in the chiral unitary model ( $\mu^{(a)} = -0.25$ ) and in the quark model ( $\mu^{(a)} = -1.2$ ) cases are shown by the lines with open squares and triangles, respectively.

they emit the more photon than the slow intermediate  $n^*$ .

## VI. SUMMARY

We have calculated the magnetic moments of the  $N(1535)$  resonance using the chiral unitary model. We have obtained the magnetic moments of the resonances as  $\mu_{n^*(1535)} \sim -0.25\mu_N$  and  $\mu_{p^*(1535)} \sim +1.1\mu_N$ . Compared with the results of  $\Lambda$  resonances in Ref. [16], the sign of the Coleman-Glashow relations (7), which comes from the SU(3) symmetry of octet, are satisfied among  $\Lambda^*(1670)$  and  $n^*(1535)$  in the chiral unitary model. This implies that  $1/2^-$  resonances are the member of an SU(3) octet. The present results qualitatively agree with the results of the constituent quark model of Ref. [17]. However, the absolute values of these results are different, so the experimental measurement will bring the information of the structure of the baryon resonances. Fi-

## Acknowledgments

We would like to thank Prof. E. Oset, for checking the calculations in detail. We would like to acknowledge Profs. M. J. Vicente Vacas and H. -Ch. Kim for useful discussions.

## APPENDIX A: LAGRANGIANS

In this appendix, we show the Lagrangians used in Sec. V to calculate the cross sections of the  $\gamma N \rightarrow \gamma\eta N$  and  $\pi N \rightarrow \gamma\eta N$  processes through the  $N^*$  intermediate state. Here  $N^*$  denotes the  $N(1535)$  resonance, which has the negative parity.

For the  $\eta NN^*$  vertex, we take the scalar coupling:

$$\mathcal{L}_{\eta NN^*} = g_\eta \bar{N} N^* + \text{h.c.} , \quad (\text{A.1})$$

where the coupling constant  $g_\eta \simeq 2.0$  is determined so as to reproduce the partial decay width  $\Gamma_{N^* \rightarrow \eta N} \simeq 75$  MeV [20] at tree level.

The transition vertex of  $N$  to  $N^*$  with one photon is given by

$$\mathcal{L}_{\gamma NN^*} = \frac{e}{4M_P} \mu_N^{(T)} \bar{N} i \gamma_5 \sigma^{\mu\nu} F_{\mu\nu} N + \text{h.c.} . \quad (\text{A.2})$$

Here we assume the isovector dominance on the transition magnetic moments  $\mu_N^{(T)}$ , and their values are given by  $\mu_p^{(T)} = -\mu_n^{(T)} = 0.68$  in units of nuclear magneton, which correspond to  $\kappa_V^* \equiv \frac{2m_N}{m_N + m_{N^*}} \mu_N^{(T)} = 0.9$  determined from analyses of eta photoproduction [30].

The  $\gamma NN$  and  $\gamma N^* N^*$  vertices have two parts, which are so-called the Dirac term and the Pauli term:

$$\begin{aligned} \mathcal{L}_{\gamma NN} = & -eQ \bar{N} \gamma_\mu A^\mu N \\ & + \frac{e}{4M_P} \kappa_N \bar{N} \sigma^{\mu\nu} F_{\mu\nu} N , \end{aligned} \quad (\text{A.3})$$

$$\begin{aligned} \mathcal{L}_{\gamma N^* N^*} = & -eQ \bar{N}^* \gamma_\mu A^\mu N^* \\ & + \frac{e}{4M_P} \kappa_{N^*} \bar{N}^* \sigma^{\mu\nu} F_{\mu\nu} N^* . \end{aligned} \quad (\text{A.4})$$

The anomalous magnetic moments of the ground state nucleons  $\kappa_N$  are used the experimental value  $\kappa_p = 1.79284739$  and  $\kappa_n = -1.9130428$  in units of nuclear magneton [20], while the anomalous magnetic moments of  $N^*$  are assumed to be  $\pm 3$  to see sensitivity of their values to the cross sections.

For the calculations of the pion-induced process, we use the following Lagrangians. The  $\pi NN^*$  vertex has the scalar type coupling, which given by

$$\mathcal{L}_{\pi NN^*} = g_{\pi NN^*} \bar{N} \vec{\tau} \cdot \vec{\pi} N^* + \text{h.c.} . \quad (\text{A.5})$$

with the coupling constant  $g_{\pi NN^*} \simeq 0.7$ , which is determined so as to reproduce the partial decay width  $\Gamma_{N^* \rightarrow \pi N} \simeq 75$  MeV [20] at tree level. The diagonal

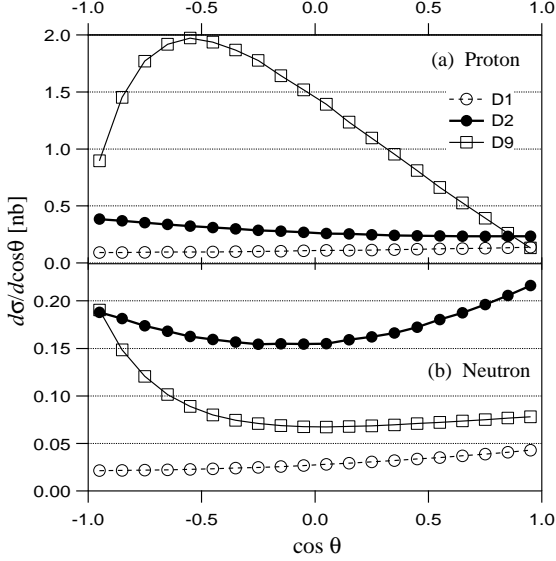


FIG. 11: Separated contributions of the dominant diagrams to the angular distribution of the emitted photon in the photon-induced process. The integration with respect to the emitted energy is performed from 80 MeV to the threshold. The lines with the open circles, black circles and squares denotes the contributions of the diagrams 1, 2, and 9, respectively.

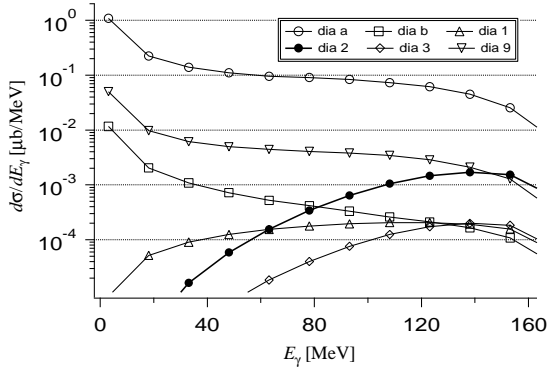


FIG. 12: Separated contributions of the dominant diagrams to the energy spectrum of the emitted photon in the pion-induced process with the initial pion energy  $E_\pi = 1000$  MeV. The lines with the open circles, squares, triangles, black circles, diamonds and down-triangles denote the contributions from the diagram  $a$ ,  $b$ , 1, 2, 3 and 9, respectively.

nally we have computed reaction cross section in order to observe the resonance magnetic moments;  $\gamma N \rightarrow \gamma\eta N$ ,  $\pi^- p \rightarrow \gamma\eta n$ . The difference in the magnetic moments is, however, not very much reflected in the bremsstrahlung processes.

vertices  $\pi NN$  and  $\pi N^* N^*$  are assumed to be here the pseudo-scalar couplings:

$$\mathcal{L}_{\pi NN} = g_{\pi NN} \bar{N} \gamma_5 \vec{\tau} \cdot \vec{\pi} N, \quad (\text{A.6})$$

$$\mathcal{L}_{\pi N^* N^*} = g_{\pi N^* N^*} \bar{N}^* \gamma_5 \vec{\tau} \cdot \vec{\pi} N^*, \quad (\text{A.7})$$

Here we use the empirical value of the  $\pi NN$  coupling  $g_{\pi NN} \simeq 13$ . For the  $\pi N^* N^*$  coupling, we assume  $g_{\pi N^* N^*} \simeq +13$ , although the sign of this coupling is important for the properties of  $N^*$ . The value of the  $\pi N^* N^*$  coupling is absolutely insensitive to the final re-

sults, since this coupling appears in the less dominant diagrams. In this formulation, we do not include the Kroll-Ruderman type diagram, since we use the scalar type coupling for the  $\pi NN^*$  vertex and it has already contain the partial contribution of the Kroll-Ruderman type vertex. The pion-photon coupling is given by

$$\mathcal{L}_{\gamma\pi\pi} = ie(\partial_\mu \pi^-)^\dagger \pi^- A^\mu - ie\pi^{-\dagger} (\partial_\mu \pi^-) A^\mu. \quad (\text{A.8})$$

- 
- [1] S. Sasaki, T. Blum, and S. Ohta, Phys. Rev. **D65**, 074503 (2002).
- [2] S. Sasaki, K. Sasaki, T. Hatsuda, and M. Asakawa, hep-lat/0209059.
- [3] Y. Nakahara, M. Asakawa, and T. Hatsuda, Phys. Rev. **D60**, 091503 (1999).
- [4] D. Jido, M. Oka, and A. Hosaka, Prog. Theor. Phys. **106**, 873 (2001).
- [5] C. DeTar and T. Kunihiro, Phys. Rev. **D39**, 2805 (1989).
- [6] D. Jido, Y. Nemoto, M. Oka, and A. Hosaka, Nucl. Phys. **A671**, 471 (2000).
- [7] N. Kaiser, P. B. Siegel, and W. Weise, Phys. Lett. **B362**, 23 (1995).
- [8] N. Kaiser, P. B. Siegel, and W. Weise, Nucl. Phys. **A594**, 325 (1995).
- [9] N. Kaiser, T. Waas, and W. Weise, Nucl. Phys. **A612**, 297 (1997).
- [10] B. Krippa, Phys. Rev. **C58**, 1333 (1998).
- [11] E. Oset and A. Ramos, Nucl. Phys. **A635**, 99 (1998).
- [12] M. F. M. Lutz and E. E. Kolomeitsev, Nucl. Phys. **A700**, 193 (2002).
- [13] T. Inoue, E. Oset, and M. J. Vicente Vacas, Phys. Rev. **C65**, 035204 (2002).
- [14] E. Oset, A. Ramos, and C. Bennhold, Phys. Lett. **B527**, 99 (2002).
- [15] A. Ramos, E. Oset, and C. Bennhold, Phys. Rev. Lett. **89**, 252001 (2002).
- [16] D. Jido, A. Hosaka, J. C. Nacher, E. Oset, and A. Ramos, Phys. Rev. **C66**, 025203 (2002).
- [17] W.-T. Chiang, S. N. Yang, M. Vanderhaeghen, and D. Drechsel, nucl-th/0211061.
- [18] B. M. K. Nefkens *et al.*, Phys. Rev. **D18**, 3911 (1978).
- [19] A. Bosshard *et al.*, Phys. Rev. **D44**, 1962 (1991).
- [20] Particle Data Group, K. Hagiwara *et al.*, Phys. Rev. **D66**, 010001 (2002).
- [21] J. A. Oller and U. G. Meissner, Phys. Lett. **B500**, 263 (2001).
- [22] U.-G. Meissner and J. A. Oller, Nucl. Phys. **A673**, 311 (2000).
- [23] U.-G. Meissner and S. Steininger, Nucl. Phys. **B499**, 349 (1997).
- [24] S. R. Coleman and S. L. Glashow, Phys. Rev. Lett. **6**, 423 (1961).
- [25] T. Hyodo, S. I. Nam, D. Jido, and A. Hosaka, nucl-th/0212026
- [26] T. Hyodo, S. I. Nam, D. Jido, and A. Hosaka, nucl-th/0305011
- [27] D. Jido, J. A. Oller, E. Oset, A. Ramos, and U. G. Meissner, nucl-th/0303062
- [28] J. C. Nacher, E. Oset, H. Toki, and A. Ramos, Phys. Lett. **B455**, 55 (1999)
- [29] D. Jido, M. Oka, and A. Hosaka, Prog. Theor. Phys. **106**, 823 (2001).
- [30] M. Benmerrouche, N. C. Mukhopadhyay, and J. F. Zhang, Phys. Rev. **D51**, 3237 (1995).